Model for Fast Evaluation of Charging Programs in the Blast Furnace

TAMOGHNA MITRA and HENRIK SAXÉN

A mathematical model for fast evaluation of charging programs in bell-less top blast furnaces is presented. The model describes the burden formation and descent procedures in the blast furnace, and can be used for designing charging programs. Experimental results in small scale were used to validate the model. The model was applied to a real charging program from a reference blast furnace. Through comparison between the estimated burden distribution and gas temperatures from an above-burden probe it was concluded that the model has captured the main features of the distribution of coke and pellets. The potential of using the model for the design of new charging programs was finally illustrated by analyzing the effect of small changes in the positions of the rings on the arising burden distribution.

DOI: 10.1007/s11663-014-0156-2

I. INTRODUCTION

DUE to increasing global competition in steelmaking and rising raw material prices, as well as a pressure to significantly decrease the emissions, the steelmaking sector faces enormous challenges in the future. For this reason, the unit processes in the chain from iron ore to finished products must be operated efficiently and without wasting primary resources. The unit process with clearly largest energy consumption in the chain is the blast furnace, where the iron oxides are reduced and melted into hot metal, which is converted to steel in the downstream basic oxygen process. The blast furnace acts are a huge counter-current heat exchanger and chemical reactor, in the upper part of which the burden (consisting of preprocessed and agglomerated iron ores as well as coke, the main energy resource) meets an ascending gas during its descent. The efficiency of the blast furnace mainly reflects how well the charged iron-bearing burden has been reduced in the upper, or lumpy, zone, as a reduction in the lower part is associated with a simultaneous consumption of coke. The primary means of controlling the conditions in the lumpy zone, including the material flows, heat and mass transfer and chemical reactions, is to control the radial distribution of the burden: Due to differences in permeability and density of the changed materials, the gas-flow distribution is largely controlled by the burden distribution. Furthermore, the burden-layer distribution plays an important role in controlling the supply of gas from the lower parts of the blast furnace to the lumpy zone through the *coke slits* in the cohesive zone, where the iron-bearing burden softens and melts. The burden distribution also controls the thermal conditions in the shaft since "ore" has about four time higher density than coke, and thus, through the thermal flow ratio, strongly affects the temperature distribution in the counter-current heat exchanging zone.

The burden distribution can be controlled by the charging equipment, which for furnaces with bell-less top means by selecting size and sequence of the material dumps, as well as the angles of the rotating chute. Often, to facilitate the decision making, the chute angles are discretized into a number of positions (typically about ten), between which the operator can choose. Still, the number of potential choices is enormous, as a charging sequence consists of 5 to 20 dumps. Furthermore, as the distribution of a ring on the burden surface depends strongly on the present burden profile, *i.e.*, on the distribution of previously charged rings, the problem is nonlinear and complex. Therefore, it is obvious that a model that can guide the operators in the choice and design of charging programs would be most welcome.

A number of investigations of the burden distribution in the blast furnace have been published,[1,2] and in many studies small-scale models have been used to shed light on the conditions.[3–6] Measurements and sampling from industrial blast furnaces have also been applied[7,8] to gain deeper understanding of the internal state. In furnaces equipped with sophisticated measurement devices, such as contact or non-contact profile meters, the burden level along a radius or diameter can be sensed after each dump. However, such devices are expensive and may require considerable maintenance and calibration in order to work properly, and high investment costs cannot justify their use in small furnaces. Furthermore, experiments in full scale are practically impossible, as the changes in the burden distribution in practice are implemented either to address a problem that has been detected (*e.g.*, excessive peripheral flow of the gas) or are dictated by gradual adjustments to achieve a goal (*e.g.*, improved gas utilization). An alternative for gaining insight into the

TAMOGHNA MITRA, Researcher, and HENRIK SAXÉN, Professor and Head of Laboratory, are with the Thermal and Flow Engineering Laboratory, Åbo Akademi University, Biskopsg. 8, 20500, Åbo, Finland. Contact e-mail: hsaxen@abo.fi
Manuscript submitted December 20, 2013.
Article published online August 12, 2014.

burden distribution is by mathematical modeling. A large number of mathematical models, ranging from data-driven approaches[9,10] to first principles models,[11,12] have been proposed. The advantage of models in the former category is that they are based on practical observations, so they reflect the true conditions, but they often require extensive measurements to which the models can be tuned. Furthermore, extrapolations may have a high degree of uncertainly. The theoretical models, in turn, have the advantage of being able to predict entirely new situations and to give deeper insight into the phenomena, but the work required for developing, and tuning, them may be considerable. Furthermore, the calculation time may be prohibitive for detailed studies of a large number of potential charging programs. An example of models of the second category with the above mentioned advantages and disadvantages are models based on the discrete element method (DEM).[3,13,14]

With the above observations in mind, a model for decision support guiding the operator in the development and choice of charging programs in blast furnaces with bell-less top has been created. Small-scale (1:10) experiments have been used to tune and verify the model. The next section of the paper illustrates the principles behind the model and the assumptions made, followed by a description of the small-scale model and its measurements in Section III. Section IV presents a comparison of between results from the experimental rig and simulations, as well as some simulation results for the full-scale case and a brief comparison of these findings with temperatures from an in-burden probe Finally, some conclusions and suggestions for future work are presented in Section V.

II. MATHEMATICAL MODEL

Figure 1 presents a flowchart outlining the working principle of the model. After entering the furnace dimensions, charging program, material properties and some simulation parameters, a base bed is initiated on which the dumps are charged. At the bottom of the simulated region, the bed is lowered in small steps, followed by descent of all layers of burden, from the bottom to the top, until the stockline descends below a given set point. This triggers the charging of the next dump, and the procedure is repeated. The following subsections present the central parts of the mathematical model, first describing the burden distribution model and then the burden descent model.

A. *Burden Distribution Model*

The burden distribution model is based on a model of the flow of the burden from a hopper to the rotating chute and onwards to the burden surface, where it forms a layer. With reference to the top part of Figure 2, the chute is assumed to be hinged at the point at which the dump leaves the down-comer from the feeding hopper. The motion of the dump is simplified by assuming the flow to be similar to that of a single particle. The dump is assumed to be stationary as it leaves the hopper, but gains speed along the down-comer to reach the exit velocity

$$v_0 = \sqrt{2g\left(h_0 + \frac{d}{\sin\alpha}\right)} \qquad [1]$$

at the end of it, where g is the acceleration due to gravity and d, h_0, and α are defined in the left part of Figure 2. After it strikes the chute, the burden is assumed to lose its velocity component perpendicular to the chute. The force balance of the particles moving down the chute at a distance x along l is given by (*cf.* insert in the left part of Figure 2)

$$a = g\sin\alpha + \omega^2 x\sin\alpha\cos\alpha - \mu\left(g\cos\alpha - \omega^2 x\sin^2\alpha\right), \qquad [2]$$

where ω is the rotation speed of the chute and μ is the friction coefficient between the material and the chute. In the simulation, the chute made one revolution in 8 seconds and the friction coefficient was fixed to be $\mu = 0.8$. The latter value was exaggerated to take into consideration the fact that a big fraction of the energy is lost when particles in the stream collide with each other. The value was found by tuning the model so that the radial position where the stream hits the burden surface agreed with values observed in small-scale experiments (see Figure 8 of Section III). Integrating the acceleration a of a particle gives its velocity at the end of the chute

$$u_0^2 = v_0^2\cos^2\alpha + \omega^2 l^2\sin\alpha(\sin\alpha + \mu\cos\alpha) + 2gl(\cos\alpha - \mu\sin\alpha) \qquad [3]$$

assuming no rolling to take place and that the only friction that occurs is between the particles and the chute. If the stock level is known at the moment when the dump is charged, one may solve the falling trajectory of the burden and use the intersection of it with the burden surface, the impact point, as the radial coordinate of the initial crest (apex) of the heap to be formed. The trajectory with reference to the axes (*cf.* Figure 2) is given by

$$y = -r^2\left(\frac{g}{2u_0^2\sin^2\alpha}\right) - r\left(\frac{1}{\tan\alpha} - \frac{gl}{u_0^2\sin\alpha}\right) - \left(\frac{gl^2}{2u_0^2} + \frac{d}{\sin\alpha}\right). \qquad [4]$$

To simplify the calculations, the surface of the (vertical cross section of the) charged dump (here numbered i) is assumed to be composed of two linear segments (*cf.* right part of Figure 2) given by

$$z_i(r) = \begin{cases} a_{1,i}r + a_{2,i} & \text{if } r \geq r_{c,i} \\ a_{3,i}r + a_{4,i} & \text{if } r < r_{c,i} \end{cases}, \qquad [5]$$

where $r_{c,i}$ is the radial coordinate of the crest, which should satisfy Eq. [4], and R_t is the throat radius of the furnace. The parameters $a_{1,i}$ and $a_{3,i}$ are defined

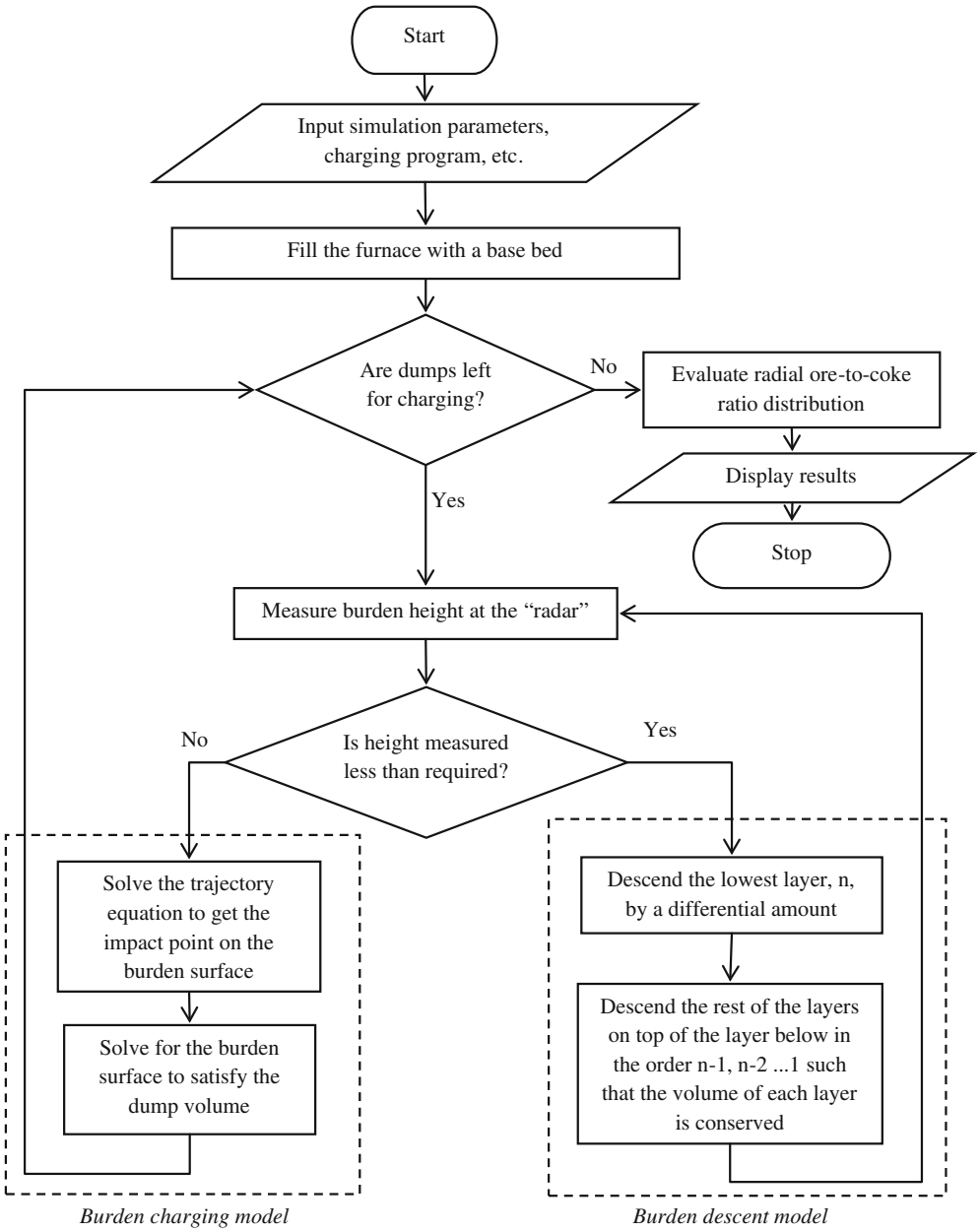

Fig. 1—Flowchart describing the mathematical model.

according to the properties (and, possibly, position) of the material charged. Typically $a_{3,i} = \tan \beta_i$, where β_i is the angle of repose of the burden in dump i, while $a_{2,i}$ and $a_{4,i}$ are determined to satisfy continuity at the crest ($a_{1,i}r_{c,i} + a_{2,i} = a_{3,i}r_{c,i} + a_{4,i}$) and the volume balance. The volume of the ith dump is given by $V_i = m_i/\rho_i$, where m is the mass and ρ is the bulk density of the material. Assuming rotational symmetry, the physical volume should be equal to the computed volume

$$V_i = \int_0^{2\pi} \int_0^R (z_i(r) - z_{i-1}(r)) r \mathrm{d}r \mathrm{d}\theta = 2\pi \int_0^R (z_i(r) - z_{i-1}(r)) r \mathrm{d}r, \quad [6]$$

where $z_i(r)$ and $z_{i-1}(r)$ are the vertical coordinates of the burden surface after and before the ith dump.

Even though the basic formulation seems simple, the consideration of the burden surface profile, $z_{i-1}(r)$, upon which the dump is charged, formed by previous rings, requires a generic algorithm that can handle arbitrary cases.[11] Common for all profiles, however, is that they consist of linear segments, limited to the radial points between the center and the wall of the furnace. Taking the location of the computed crest of the dump as the starting point, the algorithm steps left and then right to detect intersection between the lines of Eq. [5] and the previous burden surface. Naturally, the cases where the charged dump extends to the furnace center, or furnace wall, have to be detected as well.

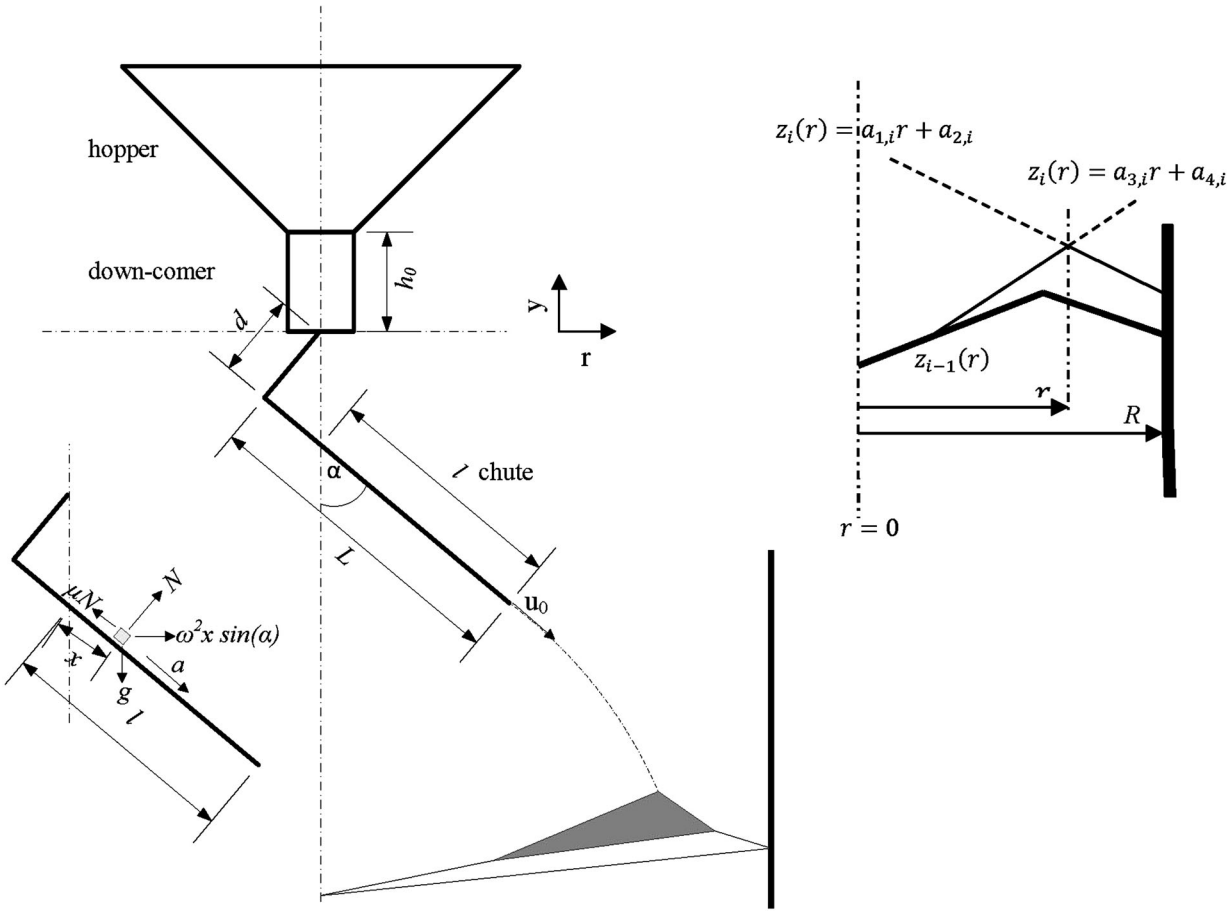

Fig. 2—Left: Schematic diagram of the burden distribution model with an inset of force balance of the particle at a point on the chute. Right: Charged layer with a crest at $r = r_{c,i}$. The burden surface before charging is depicted by the thick solid line.

Furthermore, some special cases must be considered. Figure 3 describes one such case which requires special attention during the determination of the layer surface to avoid sudden changes in the volumes while solving the problem numerically. V_{dump} is the volume of the present dump to be charged on the bed (shaded region in the figure). The top left subfigure shows the burden surfaces formed at different apex heights, h, while the top right subfigure schematically presents the volume of the formed layer at different apex heights: The aim is to find an apex height for which the volume of the layer formed equals V_{dump}. In the depicted case this is not possible, because there is an abrupt change in the layer volume for a differential change in apex height, caused by the ridge of the bed (*cf.* top left subfigure). In the illustrated case, there is no apex height h satisfying the volume balance. To avoid this problem, a break point is added where the slope of the surface of the layer is changed as indicated in the bottom subfigure of Figure 3.

B. *Burden Descent Model*

The burden descent model, by which the layers are shifted downwards between the dumps, is based on the assumption that the material bulk density and other physical properties remain uniform as the layers slowly descend through the shaft. It takes into account the increase of the diameter of the shaft, neglecting effects like pellet push and mixed layer formation.

Early experimental and modeling studies[15,16] as well as recent DEM calculations by Natsui *et al.*[6] suggest that the particles near the wall travel faster than those at the center. In the present model, the particles are assumed to maintain the relative distance from the symmetry axis, as shown schematically in Figure 4. This behavior has also been observed in small-scale experiments.[1,17]

In order to illustrate the procedure applied, Figure 5 presents a schematic description: Points 1 to 7 in the upper part of the figure represent a series of points through which the base surface runs. On this, a burden layer with the surface running through points a to e exists at time $t = t_0$. The points 3′ to 5′ and b′ to d′ are corresponding points for the surfaces on the layer and the base surfaces, respectively, on the path-lines (*cf.* Figure 4); these points are introduced to be able to study the layer thickness at all bending points. At a later time, $t = t_1$, the layer between the two surfaces has descended to a level illustrated in the lower part of the figure. The

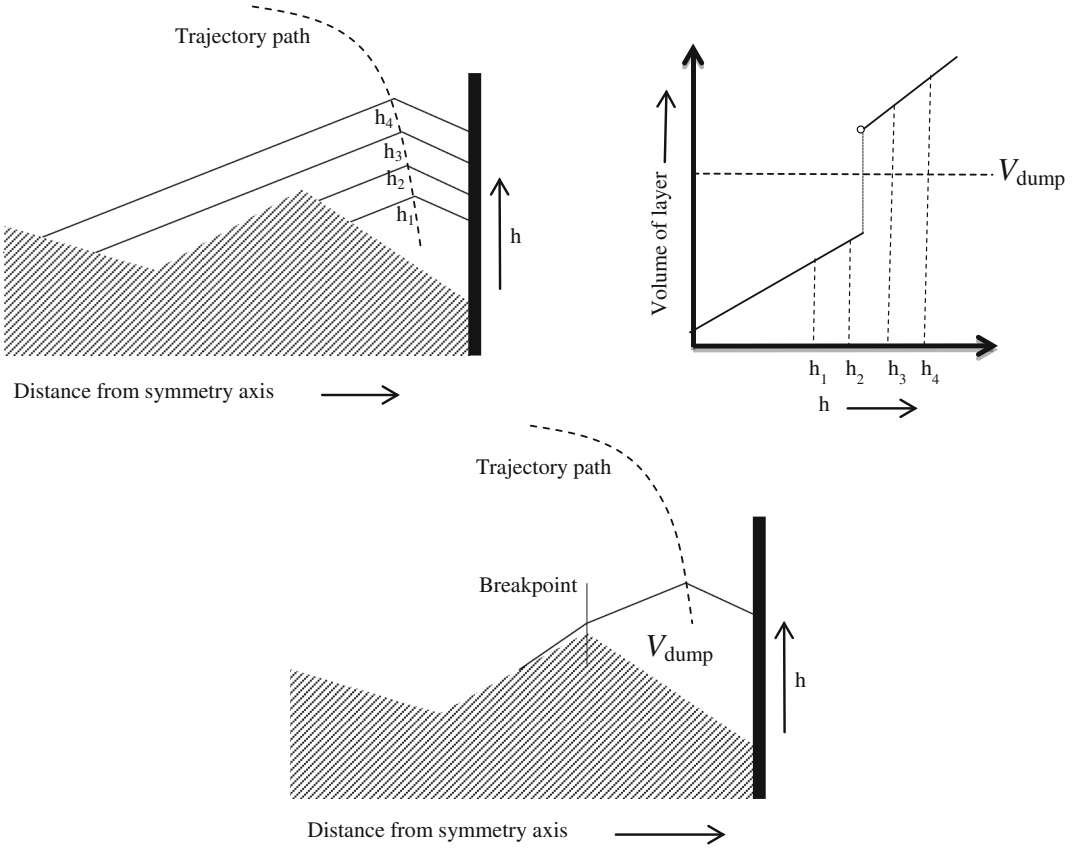

Fig. 3—Schematic of layer formation and calculated volume of the charged layer. Top: Original formulation leading to infeasible solution, as the volume of the dump (V_{dump}) cannot be satisfied. Bottom: Modified approach, where segment extending over the apex is truncated by locally increasing the repose angle at the apex, making the volume of the layer on the burden surface continuous with the apex height h.

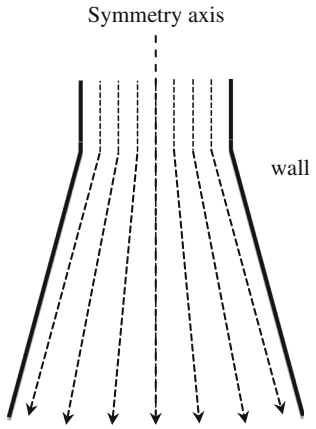

Fig. 4—Schematic diagram of the particle path.

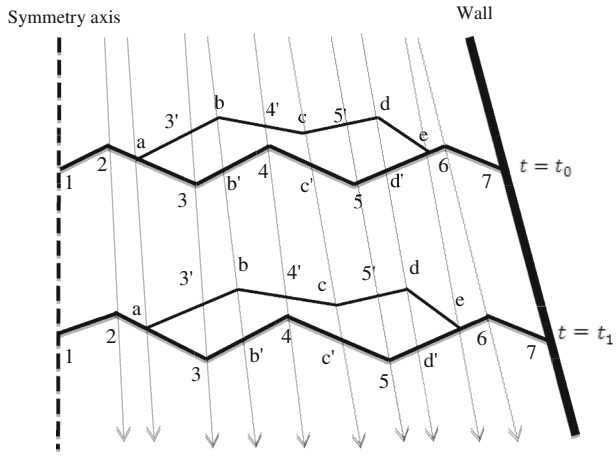

Fig. 5—Burden descent procedure. The height of a layer at every point where its limiting surfaces show a discontinuous derivative is considered to preserve the shape and volume of the layer.

points 1 to 7, 3′ to 5′, a to e, b′ to d′ are assumed to always maintain their relative position with respect to the symmetry axis, *i.e.*, to lie on the same path-line.

The points can be represented in two dimensions by (r_n, z_n), where r_n is the radial distance with respect to the symmetry axis and z_n is vertical level of the point, for $n = 1, 2, \ldots$, a, b, … and n' are the corresponding points as described earlier. In order to keep the relative radial distances equal, we have the condition

$$\left(\frac{r_n}{R_n}\right)_{t=t_0} = \left(\frac{r_n}{R_n}\right)_{t=t_1}, \quad [7]$$

$$\left(\frac{r_{n'}}{R_{n'}}\right)_{t=t_0} = \left(\frac{r_{n'}}{R_{n'}}\right)_{t=t_1}, \quad [8]$$

where R_n is the distance of the wall from the symmetry axis at z_n. The height of the layer is given by

$$h_n = \sqrt{(z_n - z_{n'})^2 + (r_n - r_{n'})^2}. \quad [9]$$

In the present model the deformation of the layer during its descent is assumed to be uniform, *i.e.*, the ratio between the layer heights at the bending points remains constant

$$(h_1 : h_2 : \ldots : h_n)_{t=t_0} = (h_1 : h_2 : \ldots : h_n)_{t=t_1}. \quad [10]$$

Therefore, for each descent step we can introduce the ratio

$$\frac{(h_n)_{t=t_0}}{(h_n)_{t=t_1}} = K. \quad [11]$$

Since the formation of mixed layers is neglected, the layer volumes at time t_0 and t_1 should remain the same

$$(V)_{t=t_0} = (V)_{t=t_1} \quad [12]$$

Thus, the points of the descended layer at time t_1 are determined numerically by requiring K to satisfy Eqs. [9], [10], and [12]. In the overall calculations, the lowermost layer is descended with a given velocity distribution. As the vertical level of burden surface at the radial coordinate for the set point has descended below a given value, a new layer is charged and the descent procedure is repeated.

In the descent model some special considerations must be taken into account regarding the changing shape of the furnace at the transition point from the throat to the shaft, where the furnace radius changes suddenly.

C. *Numerical Aspects*

The simulation model outlined above was implemented in Matlab, using a graphical user interface (GUI) to make it user-friendly. Even though the burden distribution calculation is very fast, the whole execution of the model takes between 30 seconds and 5 minutes, depending on the length of the charging program and the number of times it has to be repeated until the results represent a quasi-stationary state. The calculations are still fast enough to allow for interactive design of charging programs (*cf.* Section IV).

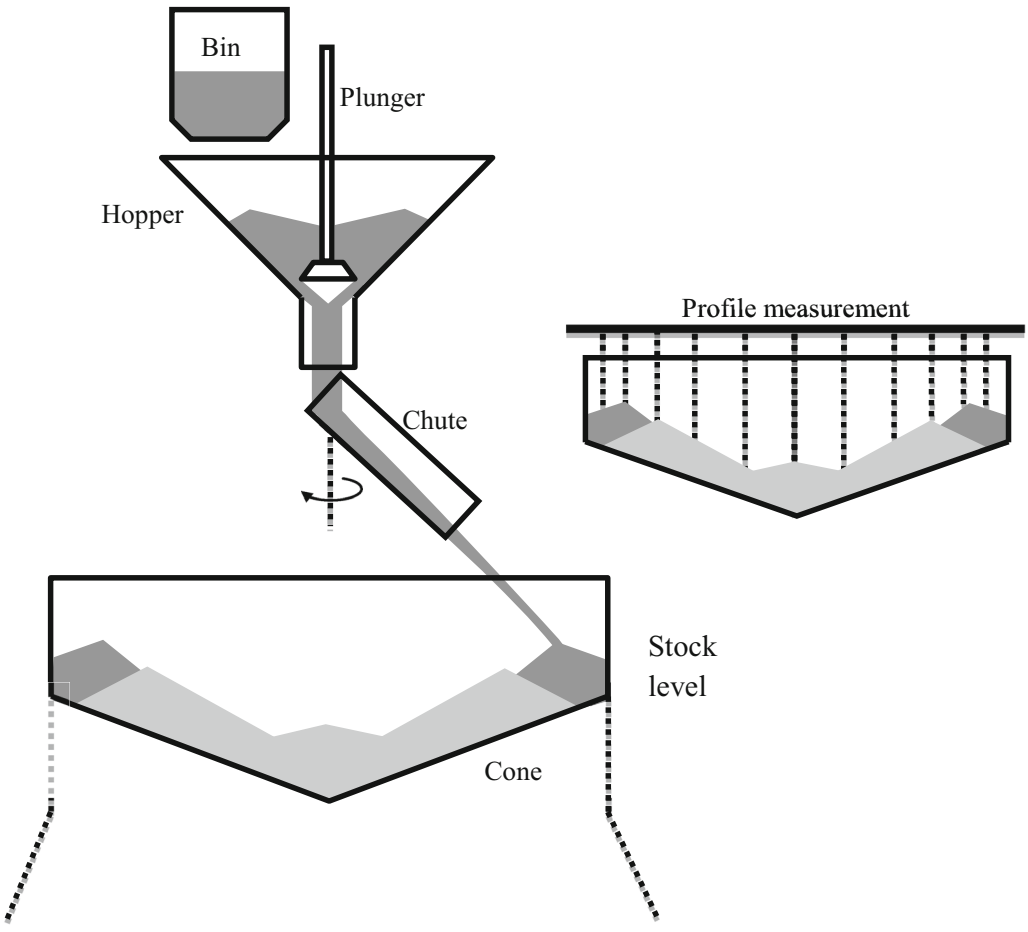

Fig. 6—Schematic diagram of the burden charging setup.

III. EXPERIMENTAL SETUP

The experimental model consists of a 1:10 scale physical model of the bell-less top burden charging apparatus with a rotating chute, schematically shown in Figure 6. The model has a throat diameter of 0.63 m and the distance between the chute tip at its lowest position and the nominal stockline is 0.2 m. The particles are scaled to 1:4 as applying the same scaling factors as for the furnace would induce unwanted effects, such as strong dust formation and unrealistic intra-particle forces. This gave a pellet size of 3 ± 1 mm and coke in the size range 5 to 20 mm and a mean size of about 15 mm. The bulk

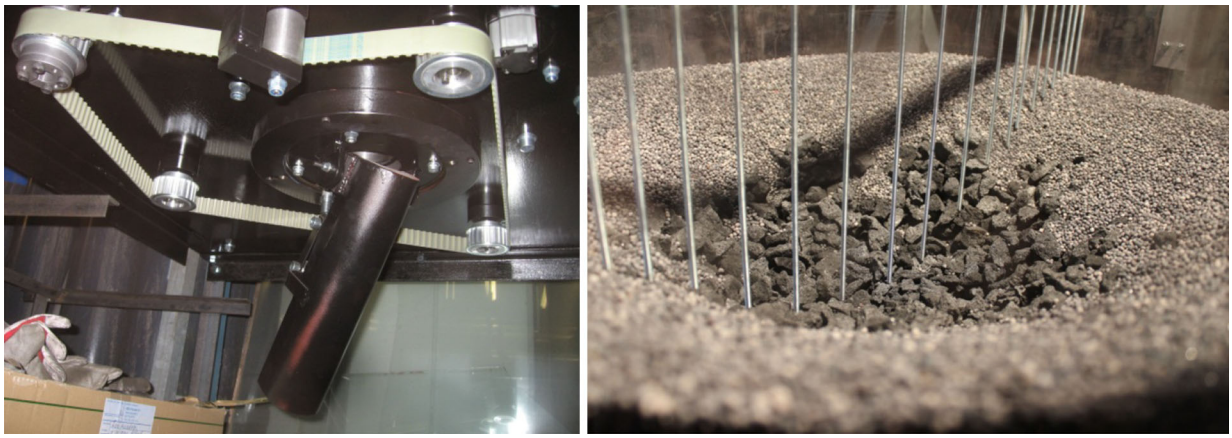

Fig. 7—Left: Small-scale model of bell-less charging. Right: Profile measurement device.

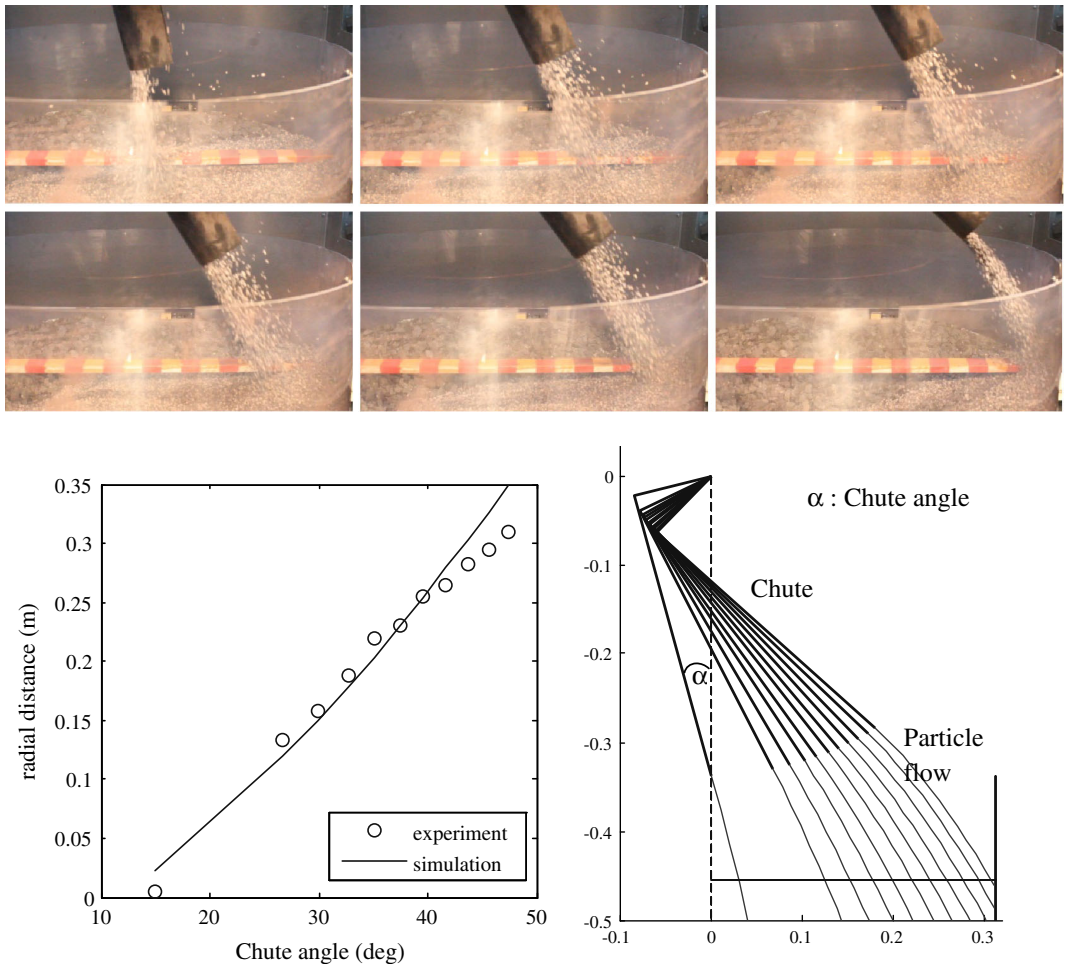

Fig. 8—Top: Flow measurements at some chute angles. Bottom: Results and calculated trajectories.

density of pellets and coke was 2150 and 500 kg/m^3 and the repose angles were 23 deg and 31 deg, respectively. A steel cone was placed into a cylindrical throat made of polycarbonate, and a layer of coke particles was glued on the cone. This mimicked a coke layer with an inclination similar to the angle of repose of coke. The bin above the hopper holds the burden until it is emptied into the hopper, where a plunger valve dictates the flow rate of particles, which fall on the rotating chute, eventually forming a ring of particles on the burden. As the density and size of the particles are different, the gap of the plunger was adjusted to create a complete ring of each type of particles. The profile measurement was carried out by a mechanical device, illustrated together with the chute in Figure 7, by which the burden-layer height at different radial coordinates was measured after charging each layer. After measuring, the "furnace" was lowered hydraulically until the aimed charging height was reached. This procedure was repeated for each charged ring of the program.

Table I. Charging Program 1: Test Program in Small-Scale Model (*cf.* Fig. 9)

Material	Chute Position	Chute Angle (deg)	Mass (kg)
Pellet	10	45.6	7.45
Coke	6	37.5	3.59
Coke	9	43.7	2.33
Coke	3	29.9	1.56
Center coke	1	15.0	0.58
Pellet	10	45.6	16.6
Pellet	10	45.6	16.6

The model of the flow from the chute was calibrated by changing the friction coefficient in the burden charging model until the impact point of the trajectories for different chute angles from the chute to a certain stock level matched the corresponding positions measured in small-scale experiments. The procedure and the results are presented in Figure 8. One may conclude that the simulation and the experimental results agree reasonably well, despite some differences for the highest chute angles.

IV. RESULTS AND DISCUSSION

A. *Small Scale*

An artificial charging program with the features of an actual charging program was created to validate the burden charging model (Table I). This is a typical

Table II. Charging Program 2: Test Program in Small-Scale Model (*cf.* Fig. 10)

Material	Chute Position	Chute Angle (deg)	Mass (kg)
Coke	9	43.7	1.7
Coke	7	39.6	1.7
Pellet	10	45.6	7.45
Pellet	9	43.7	7.45
Coke	8	41.7	1.7
Coke	6	37.5	1.7
Pellet	9	43.7	7.45
Pellet	6	37.5	7.45

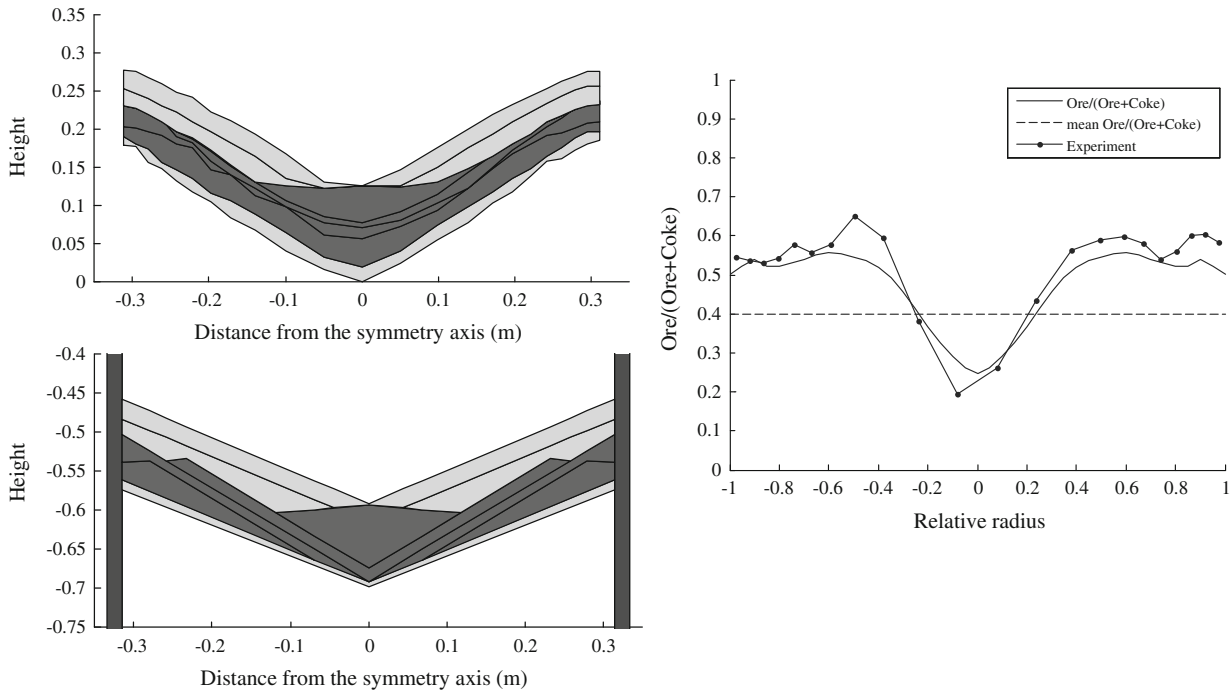

Fig. 9—Results of Charging Program 1 (*cf.* Table I). Left: Profiles measured in the experimental setup (top) and simulated results (bottom), where ore and coke are represented by light and dark layers, respectively. Right: Corresponding $O/(O + C)$ distributions.

charging program for furnaces where a locally strong central gas flow is desired. The coke is charged at medium charging angles whereas the pellets are charged near the wall. A center-coke dump between the coke and pellet charges assures enough gas flow in the center by keeping this region practically free of pellets.

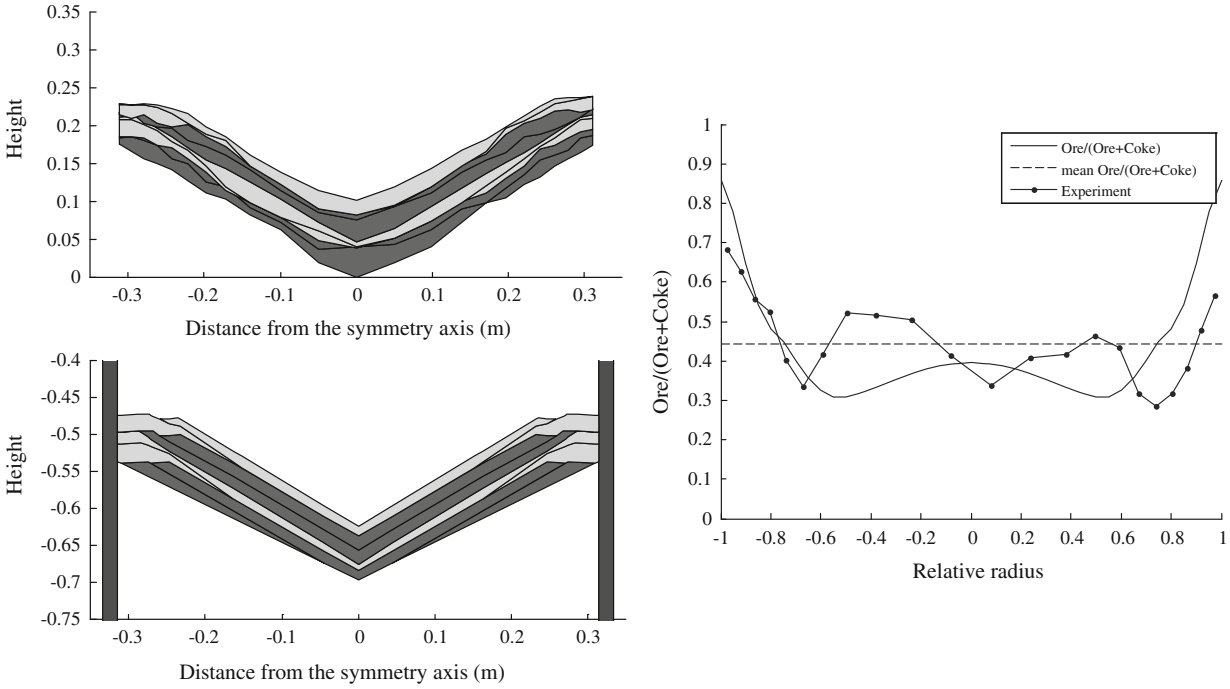

Fig. 10—Results of Charging Program 2 (*cf.* Table II). Left: Profiles measured in the experimental setup (top) and simulated results (bottom), where ore and coke are represented by light and dark layers, respectively. Right: Corresponding $O/(O + C)$ distributions.

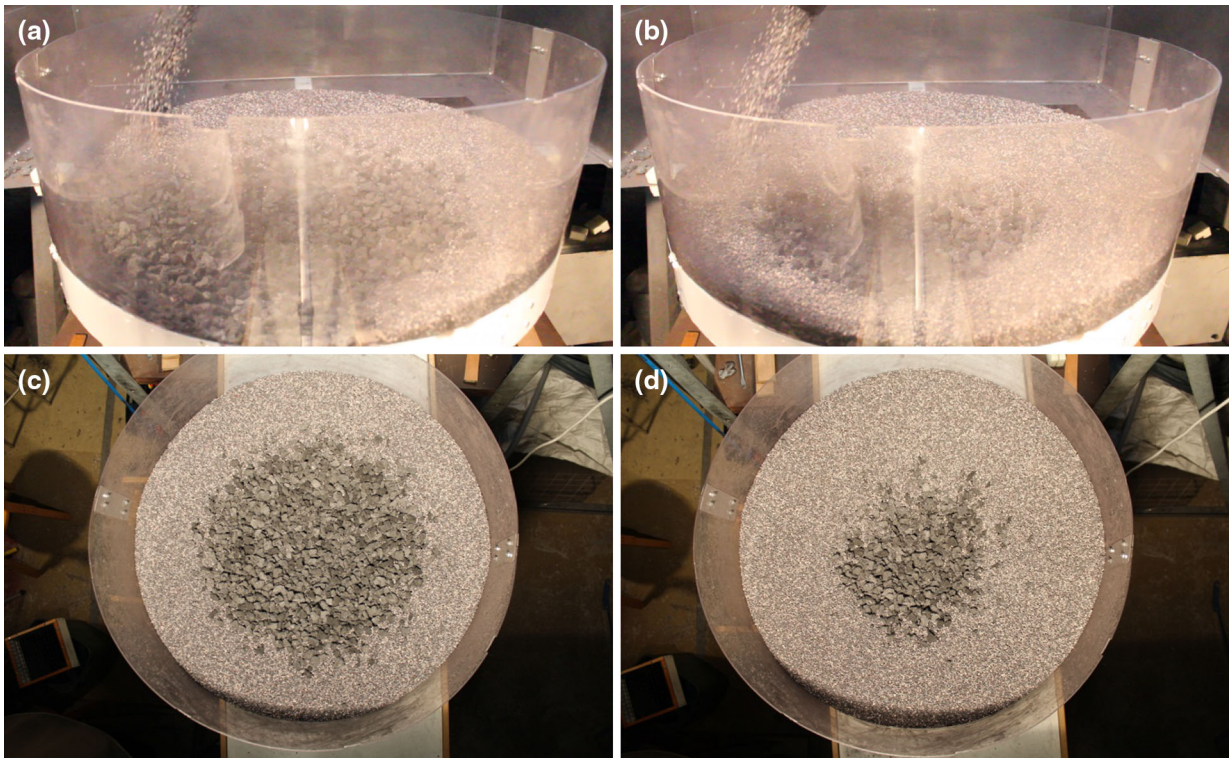

Fig. 11—Snapshots showing the sliding of a pellet layer over another. (*a*) First pellet layer (*cf.* Table II) charged at chute position 10. (*b*) Top view for the first pellet layer. (*c*) Second pellet layer (*cf.* Table II) charged at chute position 9. (b) Top view for the second pellet layer.

Table III. Charging Program 3 (c = Center, w = Wall): Simplified Version of Program Applied in the Reference Blast Furnace (*cf.* Fig. 12)

			Chute Positions										
Material	Mass (kg)	Direction	1	2	3	4	5	6	7	8	9	10	11
Coke	200	w → c									1		1
Coke	3050	w → c		1		1							
Coke	500	w → c						1		1			
Coke	3050	w → c						1		1			
Pellet	1200	w → c								1	1		
Pellet	11,200	w → c								1	1		
Coke	200	w → c										1	1
Pellet	2200	w → c										1	1
Pellet	11,200	w → c										1	1

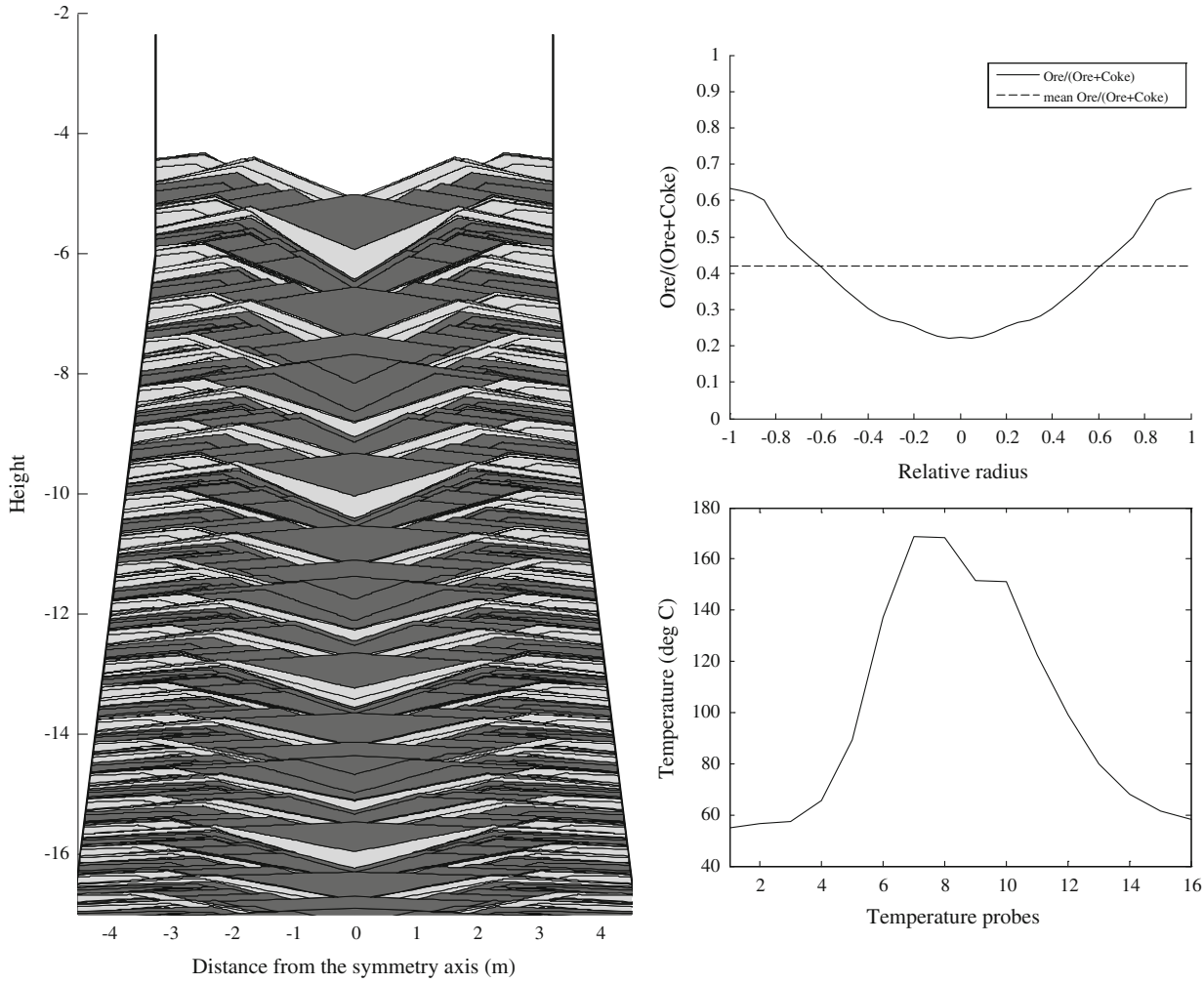

Fig. 12—Results of Charging Program 3 (cf. Table III). Left: Simulated profiles for real furnace, where ore and coke are represented by light and dark layers, respectively. Right: Simulated $O/(O + C)$ distribution (top) and temperature profile from the above-burden probe (bottom).

The results are presented in Figure 9, where the upper left and lower left subfigures correspond to the experimental and simulation results. The share of pellet along the cross-section of the bed is illustrated in the right part of the figure. Despite some differences between the results, it can be concluded that a relatively close correspondence between the simulations and the experiments has been obtained.

Longer charging programs were also tested. An example (Program 2) is given in Table II. This would be a typical charging program for furnaces where a more uniform gas distribution is desired. In this charging program both the pellet dumps were charged near the walls and the coke dumps were charged at intermediate and relatively higher angles. As seen in Figure 10, the simulation model has captured the real

situation quite well, but overestimates the pellet share at the wall. This is due to the fact that large coke particles segregate from the apex of the coke rings and roll toward the walls. The discrepancy observed in the center, where the model underestimates the share of pellets, is due to the fact that the second pellet layer slid over the first one and entered into the center region, which could clearly be observed on the videos taken during the experiment. This is seen in the picture series of Figure 11.

B. *Full Scale*

1. *Estimation based on a real charging program*

A charging program in full scale from a reference blast furnace was simulated using the model. The

Table IV. Charging Program 4 (c = Center, w = Wall): The Effect of the Order of the Ring Charged in Dump Two is Studied in Fig. 13

			Chute Positions										
Material	Mass (kg)	Direction	1	2	3	4	5	6	7	8	9	10	11
Coke	3350	c → w	1			1		1					
Coke	3350	w → c/c → w						1	1		1		
Pellet	13,000	w → c					1	1					
Pellet	13,000	w → c										1	1

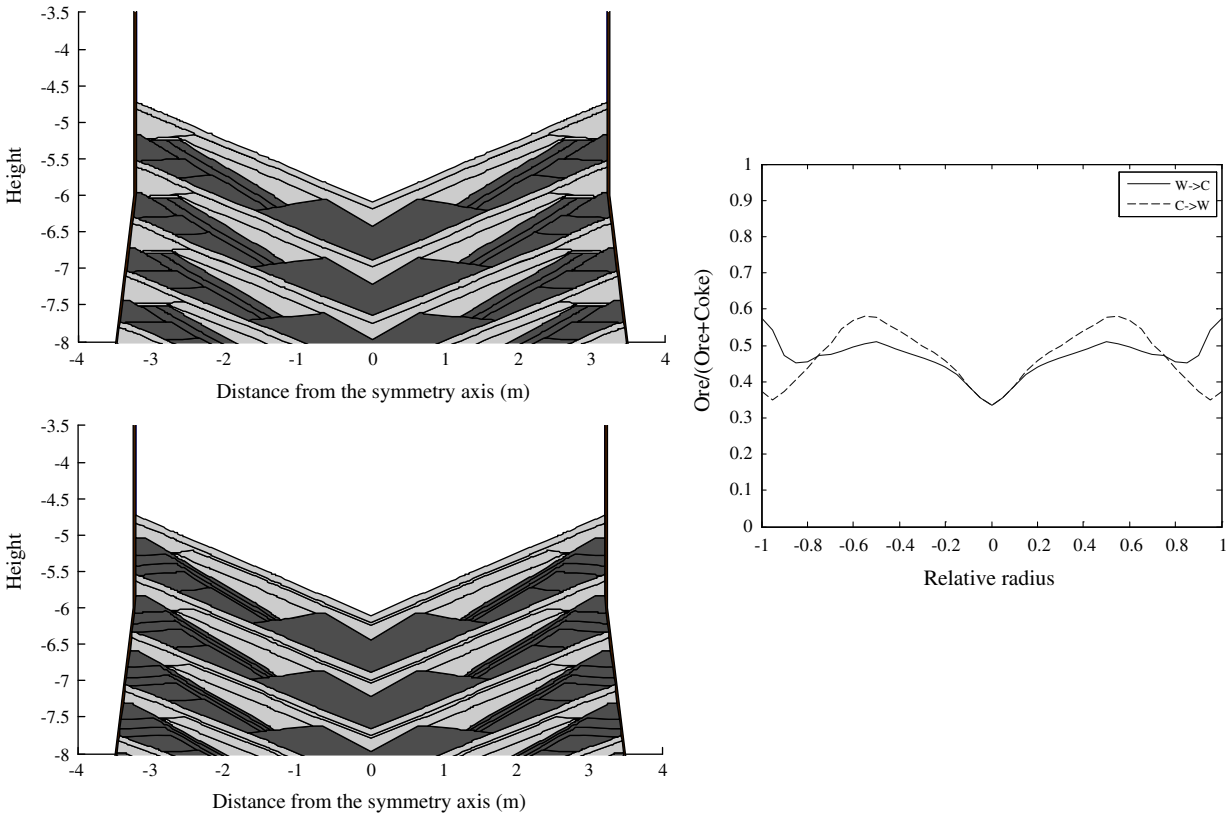

Fig. 13—Simulation of Charging Program 4 (*cf.* Table IV). Left: Rings of the second coke dump were charged from wall to center (top) or from center to wall (bottom). Right: Corresponding $O/(O + C)$ distributions.

Table V. Charging Program 5 (c = Center, w = Wall): Parentheses Denote Ring Positions That are Altered (*cf.* Figure 14)

			Chute Positions										
Material	Mass (kg)	Direction	1	2	3	4	5	6	7	8	9	10	11
Coke	3350	c → w	1			1		1					
Coke	3350	w → c		(1)				(1)	1		1		
Pellet	13,000	w → c					1	1					
Pellet	13,000	w → c										1	1

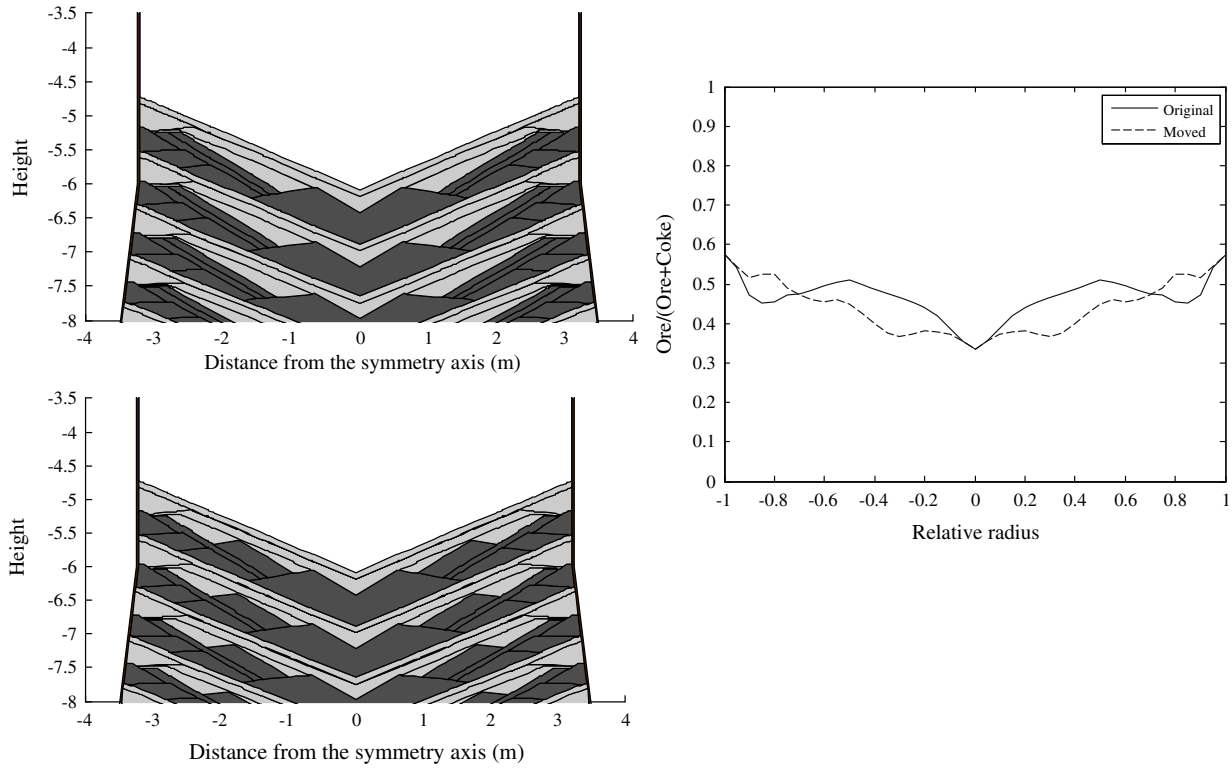

Fig. 14—Simulation of Charging Program 5 (*cf.* Table V). Left: The last ring of the second coke dump was changed from chute position 6 (top panel) to position 2 (bottom panel). Right: Corresponding $O/(O + C)$ distributions.

reference is an 1100 m^3 blast furnace with a throat and hearth diameters of 6.3 and 7.5 m, which uses pellets as the iron-bearing material. During the period studied it was operated at an ore-to-coke ratio of about $O/C = 0.72$ (*i.e.*, $O/(O + C) = 0.42$). The charging program chosen for illustration was fairly complex with more than 120 rings, but a general outline of it is given in Table III, where the lower indices of the chute give rings closer to the furnace center. In this charging program most of the ore is charged at higher angles and the coke is charged at the center, but some coke is charged at the walls to prevent complete loss of permeability due to thick ore layers. This is also evident from the calculated $O/(O + C)$ distribution profile (Figure 12, right top subpanel).

The left panel of Figure 12 illustrates the simulated burden distribution. As the furnace lacks profile-sensing devices, a direct comparison of the simulated and true results is not possible. Instead, an indirect approach was made: The gas temperatures measured at 8 + 8 points along the throat diagonal by an above-burden probe was used to illustrate the gas-flow distribution: Regions where coke dominates are expected to show a stronger gas flow and the cooling of the gas along its descent is less because the coke is much lighter than pellets.[18] As can be seen in the right part of Figure 12, the simulated $O/(O + C)$ ratio is almost a mirror image of the gas temperature, which indicates that the simulated distribution is in general agreement with the measurements.

2. *Design of new charging programs*

In order to illustrate the usefulness of the model, its application to charging program design is next illustrated. By using the model, the blast furnace operator can flexibly study the formation of ore and coke layers in the furnace, *e.g.*, with the coke slits in the cohesive zone in mind, the effect of the order in which the rings are charged (*e.g.*, from wall to center or center to wall), the formation of crests which prevent material with lower repose angles (pellets) from entering the central parts of the furnace, center-coke charging philosophy, *etc.*

Table IV shows a charging program where individual dumps of coke and pellet are divided into three and two rings each. These rings may be charged from the wall to the center (w → c) or from the center to the wall (c → w): Such small changes may cause big differences in the resulting burden distribution. To demonstrate this, the rings of the second coke dump were charged in the two alternatives $9 \rightarrow 7 \rightarrow 6$ and $6 \rightarrow 7 \rightarrow 9$. Figure 13 illustrates the significant effect of the direction of charging. The reason is that in the case of w → c charging, a pocket is created by the coke layers which traps the pellet, leading to a higher ore fraction at the wall. When the direction of rings is reversed, *i.e.*, c → w, no such pocket is formed and the share of coke at the wall increases.

Charging Program 5 (Table V) is another illustration example of that even a minor change of the program may cause large changes in the burden distri-

bution. In this case the last ring of the second dump was changed from chute position 6 to position 2. This led to more uniform coke distribution along the radius yielding a lower ore ratio at the center, as shown in Figure 14.

V. CONCLUSIONS

A simulation model for fast evaluation of charging programs in blast furnaces with bell-less tops has been developed. The model is based on a simplified treatment of the burden formation and descent procedures in the blast furnace. Comparing experiments in a 1:10 pilot rig with the model's results, a reasonable agreement was found, indicating that the simulation model has sufficient accuracy. The model was next applied to a charging program from an industrial blast furnace. Comparing the estimated burden distribution with gas temperatures measured at an above-burden probe along the throat diagonal it was concluded that high gas temperatures corresponded with a high coke ratio in the bed, while regions where the bed consisted of mainly pellets showed low gas temperatures. This indicated that the model had captured the main features of the true burden distribution.

The most useful feature of the model is its potential in designing new charging programs for the blast furnace. Since the layer-forming progress on the burden surface is complex and is affected by not only the chute position but also the present burden surface profile and the charging, the fast and interactive evaluation tool developed makes it possible for the operators gain deeper insight into the charging progress and its effect on the layer thickness distribution in the bed.

As for future developments of the model, the layer distributions predicted by the model could be made more realistic by splitting each ring into several parts, mimicking the different trajectories of the burden in the stream from the chute. Further developments would be to consider mechanisms such as pellet push and percolation, by including mixed layers in the simulation. The model will also be used as a basis for an estimation of the gas distribution in the lumpy zone, which would make it possible to validate its results using information from above-burden or in-burden probes.

ACKNOWLEDGMENTS

The authors would like to acknowledge M.Sc. Simon Renlund and M.Sc. Mathias Sundqvist for experimental work with the small-scale charging model. We would also like to thank the Graduate School of Chemical Engineering, the Akademi of Finland, and FIMECC and its ELEMET and SIMP programs, with financial support from Tekes and participating companies, for funding this work.

REFERENCES

1. J.I. Park, H.J. Jung, M.K. Jo, H.S. Oh, and J.W. Han: *Met. Mater. Int.*, 2011, vol. 17, pp. 485–96.
2. Z. Fan, S. Natsui, S. Ueda, T. Yang, J. Kano, R. Inoue, and T. Ariyama: *ISIJ Int.*, 2010, vol. 50, pp. 946–53.
3. H. Mio, S. Komatsuki, M. Akashi, A. Shimosaka, Y. Shirakawa, J. Hidaka, M. Kadowaki, S. Matsuzaki, and K. Kunitomo: *ISIJ Int.*, 2008, vol. 48, pp. 1696–703.
4. C.K. Ho, S.M. Wu, H.P. Zhu, A.B. Yu, and S.T. Tsai: *Miner. Eng.*, 2009, vol. 22, pp. 986–94.
5. J. Jimenez, J. Mochon, A. Formoso, and J.S. De Ayala: *ISIJ Int.*, 2000, vol. 40, pp. 114–20.
6. S. Natsui, S. Ueda, H. Nogami, J. Kano, R. Inoue, and T. Ariyama: *Steel Res. Int.*, 2011, vol. 82, pp. 964–71.
7. Q. Zhu, C. Lu, Y. Yin, and X. Chen: *J. Iron Steel Res. Int.*, 2013, vol. 20, pp. 33–37.
8. S. Nag and V.M. Koranne: *Ironmaking Steelmaking*, 2009, vol. 36, pp. 371–78.
9. Y. Kajiwara, T. Jimbo, and A. Kometani: *Trans. ISIJ*, 1984, vol. 24, pp. 379–86.
10. J. Hinnelä and H. Saxén: *ISIJ Int.*, 2001, vol. 41, pp. 142–50.
11. H. Saxén and J. Hinnelä: *Miner. Process. Extr. Metall. Rev.*, 2004, vol. 25, pp. 1–27.
12. V.R. Radhakrishnan and K.M. Ram: *J. Process Control*, 2001, vol. 11, pp. 565–86.
13. T. Nouchi, M. Sato, and K. Takeda: *JFE Tech. Rep.*, 2009, vol. 13, pp. 28–33.
14. Y. Yu and H. Saxén: *Chem. Eng. Sci.*, 2011, vol. 65, pp. 5237–50.
15. J. Yagi: *ISIJ Int.*, 1993, vol. 33, pp. 619–39.
16. M. Ichida, K. Nishihara, K. Tamura, M. Sugata, and H. Ono: *ISIJ Int.*, 1991, vol. 31, pp. 505–514.
17. M. Ichida, K. Anan, M. Takao, K. Kakiuchi, Y. Morizane, I. Yamada, and T. Nakayama: *Nippon Steel Tech. Rep.*, 2006, vol. 94, pp. 80–86.
18. J.J. Poveromo: *Iron Steelmaker*, 1995–1996, vol. 22–23.